Making Non-Volatile Nanomagnet Logic Non-Volatile

Aaron Dingler*[1], Steve Kurtz*[1], Michael Niemier[1], Xiaobo Sharon Hu[1], Gyorgy Csaba[2], Joseph Nahas[1], Wolfgang Porod[2], Gary Bernstein[2], Peng Li[2], Vjiay Karthik Sankar[2]
University of Notre Dame Departments of Computer Science and Engineering[1], and Electrical Engineering[2]
{adingler, skurtz, mniemier, shu, gcsaba, jnahas, porod, bernstein.1, pli, vsankar}@nd.edu

ABSTRACT

Field-coupled nanomagnets can offer significant energy savings at iso-performance versus CMOS equivalents. Magnetic logic could be integrated with CMOS, operate in environments that CMOS cannot, and retain state without power. Clocking requirements lead to inherently pipelined circuits, and high throughput further improves application-level performance. However, bit conflicts – *that will occur in defect free, pipelined ensembles* – can make non-volatile logic volatile. Assuming a field-based clock, we present hardware designs to improve steady state non-volatility, and explain how design enhancements could increase clock energy. We then suggest materials-related design levers that could simultaneously deliver non-volatility and low clock energy.

Categories and Subject Descriptors

B.6.1 [**Design Styles**]: *Cellular arrays and automata,* B.8.2 [**Performance and Reliability**]: *Performance Analysis and Design Aids*

General Terms

Performance, Design, Reliability

Keywords

Nanomagnet logic, nanotechnology, NML, MQCA

1. INTRODUCTION

Many device technologies are being developed in an effort to replace or augment CMOS, as both the size and performance scaling trends associated with Moore's Law are becoming more difficult to achieve. Per the ITRS, nanomagnet logic (NML) uses device-to-device coupling between lithographically defined magnets, with nanometer feature sizes, to perform Boolean logic operations. Potential advantages of NML include extremely low power information processing, the ability to function in harsh environments, and non-volatility (even at the gate level).

NML is commonly compared to subthreshold CMOS where the focus is on optimizing power over speed ([1]). This is more poignant because of the upper limit (~1Ghz) on NML speeds as dictated by magnetic reversal times. **Active energy** associated with an NML-based computation could be 96 times less than a CMOS equivalent – even after accounting for clock overhead [2, 3]. With the exception of any drive circuitry, standby power should be 0.

NML could process information robustly in **harsh environments**. Notably, magnetic devices are intrinsically radiation hard. Experimental results by our group (not yet published) have considered NML ensembles that were subjected to radiation doses of up to 10 Mrad. No state change was observed post-dose, and follow-on switching experiments are planned. Additionally, devices could retain their magnetic properties below the Curie temperature of a material (e.g., 1100º C for Co), and operate equally well at cryogenic temperatures.

In principle, NML ensembles should be **non-volatile** (NV). At the application-level, this is beneficial for multiple reasons. **(i)** With supply voltage scaling, leakage power rivals dynamic power in state-of-the-art CMOS, and magnetic logic devices could mitigate standby power. As examples, [4] proposed using STT-RAM based lookup tables for both memory and combinational logic in multi-core processors, which could reduce chip-level power by 70%. [5, 6] proposed using magnetic tunnel junctions (MTJs) as tunable resistors to implement gate-level storage in dynamic current mode logic (DyCML). [6] considered a DyCML adder where one input took the form of an MTJ. For applications such as a sum of absolute differences (e.g., common in MPEG encoding for motion detection), pattern matching [7], etc., a given input can change infrequently and be stored at the gate. The benefit of NML over other approaches of this sort is that both logic and storage can be accomplished in NML. Thus, storage is intrinsic to the logic and no read/write penalties are incurred. Furthermore, this can simplify the manufacturing process. **(ii)** Systems with unreliable power supplies could also benefit. While computational state could be backed up to NV storage in the event of a power failure – and restored when power is restored – gate level state should be preserved in NML ensembles, as the logic devices themselves are magnetic. Thus, hardware for wireless applications (e.g., RFID), hardware that relies on energy scavenging, etc., could benefit. **(iii)** While closely related to (ii), any logic should be instant off/instant on – and computation could resume whenever power is restored.

For an NML circuit to be truly NV, *every* magnet should maintain its state when computation ceases. Therefore, the energy difference between magnetization states should be on the order of N kT, where N (typically 40-60) is determined by the number of devices and how long one wishes information to be preserved. While steady state stability is a function of a given device's size, shape, and material, it can also be affected by the state of neighboring devices – and may be threatened by inherent pipelining even if circuits are defect free. Here, we consider tradeoffs between design enhancements to preserve information post computation, and clock energy.

After discussing relevant background regarding the experimental state-of-the-art related to both NML ensembles and clocking (**Sec. 2**), we will discuss our technical contributions in more detail.

In **Sec. 3**, we show that even circuits that are free of hard errors (e.g., from fabrication variation [8]) and soft errors (e.g., from thermal noise [9]) are at risk of losing information in the steady state. Bit conflicts (e.g., an anti-ferromagnetic (AF) line with state ↑↓↓↑↓ instead of ↑↓↑↓↑) that might occur due to soft errors can initiate "random walks" that can destroy the state of an NML ensemble post re-evaluation [10]. Regardless of clock mechanism, bit conflicts are unavoidable in error free, inherently pipelined NML. Also, structures proposed in previous work (e.g., [2]) that

*Both A Dingler and S Kurtz contributed equally to this work, are listed alphabetically, and should be considered co-first authors.

DAC 2012, June 3-7, 2012, San Francisco, California, USA.

could operate with acceptably low energy clocks may not retain state as computation ceases. We discuss stability qualitatively and quantitatively, and identify two approaches to improve stability.

Using a field-based clock as context, in **Sec. 4**, we discuss design changes (i.e., to magnet aspect ratio, thickness, etc.) to enhance steady state stability in ensembles of polycrystalline devices. Case studies (i) quantify clock energy overhead, (ii) demonstrate correct operation, and (iii) illustrate that stability can be improved despite thermal noise. However, increased stability will (not surprisingly) come at the cost of higher clock energy. To reduce clock energy to acceptable levels, and enable pipelined ensembles with improved steady state stability, in **Sec. 5**, we discuss the benefits of materials-centric design levers – enhanced permeability dielectrics (EPDs) [11] (to more efficiently generate clock fields) and biaxial anisotropy [9] (originally suggested for preserving hard axis stability during ensemble re-evaluation). New experiments with EPDs and consideration of clock field requirements for biaxial devices are presented. Notably, biaxial devices could lead to NV NML with just a 2-5X increase in clock energy (with no other design enhancements). **Sec. 6** conclues.

2. BACKGROUND

2.1 Devices, gates, and interconnect

Single domain magnets can represent and store binary data. Ensembles of magnets can also move and process information. A "wire" (Fig. 1) can be formed from a line of magnets that are anti-ferromagnetically coupled with each other. Ferromagnetic (F) interconnect is also possible [12]. A functionally complete logic set can be realized with combinations of majority voting gates. By setting one input to a logic '0' or '1', the gate can execute a NAND/NOR (or AND/OR) function [13]. This "parts library" has been expanded to include programmable majority gates, fanout, and non-majority AND/OR logic [8].

2.2 Field-driven clocking

Externally supplied switching energy is needed to re-evaluate a magnet ensemble (e.g., Fig. 1a) with new inputs (Fig. 1b,c) to overcome (i) both the intrinsic demagnetizing energy barrier (EB) (Fig. 2a), and (ii) any Zeeman energies contributed by fringing fields from neighboring magnets that reinforce the original state.

To modulate the EBs of magnet ensembles "on-chip," [14] proposed using hard axis directed magnetic fields from current driven wires. Clock energy could be amortized over 100,000s of devices as a single clock line could control many parallel ensembles. Clock lines can be placed in series and in multiple planes to minimize driver overhead [8]. Fringing fields from devices themselves also help with the transition to a 0º state (Fig. 2b). As such, the magnitude of the required clock field (and current) need not be excessively high [2, 14]. If a driving neighbor provides a y-directed field, a target magnet's energy landscape shifts (Fig. 2c), and it rotates toward a preferred easy axis (while the clock is applied). When the clock is removed, the magnets will completely relax to a new, low energy ground state (Fig. 1c).

[14] proposed CMOS compatible clocks that have been (i) fabricated [15], (ii) used to switch the state of individual magnetic islands [15], and (iii) used to re-evaluate line and gate structures with new inputs [16]. Looking to larger systems, parallel ensembles of magnets over a given wire (Fig. 1d) could (a) rest in a ground state to drive a second, adjacent group (i.e., N-1 drives N in Fig. 1b), (b) be placed into the metastable, 0º state required for re-evaluation, (Fig. 1b, Fig. 2b), or (c) relax into a new ground state (Fig. 1c) thus transmitting information. Devices controlled

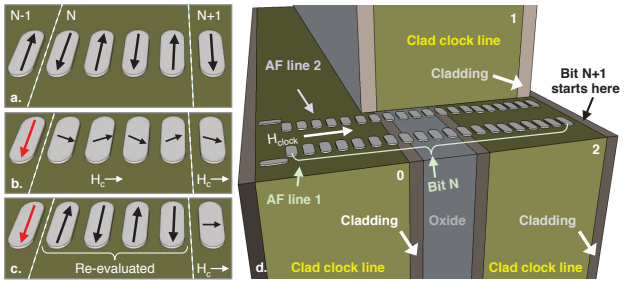

Figure 1: (a) AF-lines move information; (b) an AF-line has a new input, and an external clocking field is used to facilitate re-evaluation of the line; (c) as the field is removed, devices relax along their easy axes; (d) clock lines control many devices, and create an inherent pipeline.

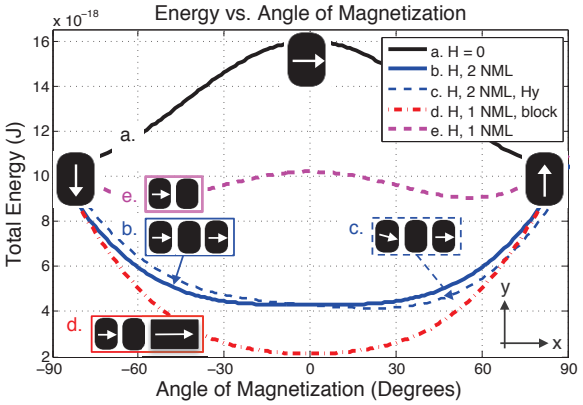

Figure 2: Energy landscape for a 60x90x30 nm^3 supermalloy device (a) with clock fields (H) equal to 0; (b) when device is subjected to a clock and fringing fields from 2 neighbors (NML) at 0º; (c) if a neighbor provides a y-bias; (d) a block mimics a neighbor in a 0º state; (e) a device coupled to just one other is in a high energy state when hard-axis biased at 0º.

by a third wire could be hard axis biased to prevent the second group from being driven from two directions (group N+1 in Fig. 1b). This ensures unidirectional dataflow, and creates an inherent pipeline. (In simulations, we employ a block of magnetic material whose easy axis is parallel to the direction of the clock field to mimic this effect – note the similarities between Fig. 2d and Fig. 2b – and avoid the high-energy state at 0º in Fig. 2e.)

2.3 Alternative clocking mechanisms

Multiferroics [17], magnetostriction [18], and STT have also been proposed as NML clocks. While a potential disadvantage of the aforementioned clocks is that every device may need to be contacted individually, potential advantages include additional energy reductions [18], and more fine-grained control of an NML ensemble (useful architecturally per [7]). However, any circuit will still be inherently pipelined [18], bit conflicts can still occur, and our insights are relevant to other clocking approaches too.

3. ORIGINS OF ENSEMBLE VOLATILITY

Non-volatility in NML has largely been quantified by considering the EB of a single device in isolation. However, device-to-device coupling will also affect a circuit ensemble's overall stability.

To begin, consider work published in [10] – which suggests that NML devices could operate near thermal equilibrium *without* the assistance of externally applied magnetic fields. [10] initially considered micromagnetic simulations of 60x120x5 nm^3 devices with a device-to-device spacing of 20 nm. This line was initialized

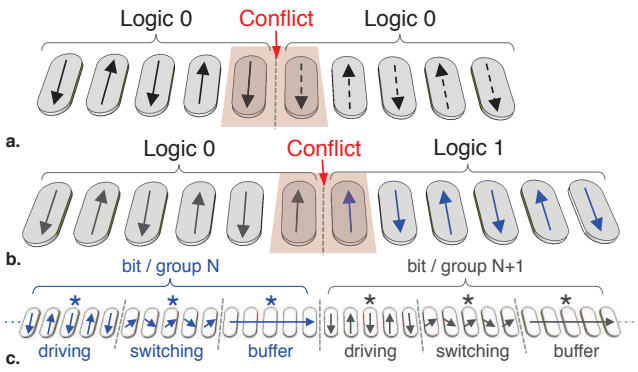

Figure 3: Conflicts occur if (a) an odd number of magnets per clock group or (b) an even number of magnets per clock group is used; (c) bit definition in an AF-line (3-phase clock).

such that all devices were initially in a 0º, metastable state, and *was* subjected to a hard axis magnetic field (37 mT) such that the EB between ↑ and ↓ states was less than the thermal energy kT. While all devices in the line relaxed to a magnetization state defined by an easy axis (i.e., ↑ or ↓), thermal noise caused some devices in the line to switch prematurely. The net result was a line with defects (where "defect" suggests improper signal ordering – e.g., ↑↓↓↑↓ – rather than manufacturing variation). With continued application of the critical switching field, said defects began to randomly walk through the line (i.e., ↑↓↓↑↓ might change to ↑↓↑↑↓, etc.) until all mis-orderings were eventually annihilated. This phenomenon was repeated experimentally where temperature elevations alone induced bit flips (detected by photoemission electron microscopy). In essence, conflicts migrated, and in turn changed the state of surrounding devices.

3.1 Impact of bit conflicts in the steady state

Clocked NML is usually inherently pipelined (e.g., see Fig. 1d, [18], etc.). While this improves throughput, pipelining will lead to bit conflicts during error free operation (i.e., even with no premature switching). Consider a line clock where an odd number of magnets span the width of each line. From Fig. 3a, if a group stores a binary 0, and an adjacent group also stores a binary 0, there cannot be complete AF ordering in the ensemble. Similarly, if an even number of magnets spans each group, a binary 1 next to a binary 0 also results in a steady state conflict (Figure 3b).

To see the potential impact of conflicts in pipelined circuits, we initially discuss micromagnetic simulations of a line of 40, 40x60x20 nm^3 supermalloy magnets spaced 8 nm apart. We use the OOMMF LLG solver [19] to model device interactions. Thermal noise is modeled with random fields, whose strength is a function of temperature, that are applied to each mesh point for each simulation time step. Note that lines of 40x60x20 nm^3 magnets with 8 nm between devices (i) allow for a reasonable comparison to 15 nm CMOS when considering minimum feature size, (ii) should not be superparamagnetic, (iii) could be controlled by a line clock with non-uniform field distributions [2], and (iv) the currents required to generate sufficiently high clocking fields should allow for clock energy budgets to make NML competitive with low power CMOS equivalents [2, 7].

In our simulations, fields were applied to groups of 5 magnets to create a pipelined, AF-line. (With a 3-phase clock, the line could store 3 bits of information as suggested by a subset in Fig. 3c.) Simulations at both 0 and 300 K suggest that multiple bits can simultaneously move through the line in a pipelined fashion, and (as in [2]) a 5 mT clock field was sufficient for re-evaluation. Now, consider the state of this line of magnets if adjacent magnet groups contain logic 0s. With this correct "architectural state", bit conflicts occur. Lines with this conflict state were again considered via OOMMF simulation. No hard axis fields were applied, and the ensemble was only subjected to the effects of thermal noise representative of a 300K environment. In all simulations, random walks occurred. As an example, after approximately 15 ns, the final state of the 40 magnet line that originally contained conflicts is a completely AF-ordered line, and information originally contained in the line is lost. Simulations of other devices/spacing (e.g., 60x90x30 nm^3 magnets with 10 nm spacing) also exhibit state-destroying random walks.

3.2 Quantifying ensemble stability

For a given device size/spacing, field coupling and thermal noise *alone* could be sufficient to initiate a state destroying random walk. To design pipelined ensembles that preserve state, we must quantify ensemble stability. While it is relatively simple to consider the stability of a device in isolation, the task becomes much more difficult when multiple coupled devices are introduced. At any moment, the stability of a single magnet depends not only on the device's intrinsic EB, but also on the fringing fields from neighboring devices – which continually change due to the effects of thermal noise.

We present an approach for predicting the stability of subcomponents within an ensemble. This will be used to evaluate design space enhancements to preserve steady state stability. Enhancements can then be studied via simulation to estimate the potential impact on clock energy (Sec. 4). (Promising design candidates can then be fed to experimentalists to significantly narrow the design space for temperature-accelerated experiments.)

To estimate ensemble stability, we introduce a simulation-based approach that considers 3-magnet ensembles where a "target" device is subjected to fringing fields from two neighboring devices. Consideration of just three devices is sufficient as conflicts are local to groups of this size (e.g., conflicts can be ↑↓↓, ↓↓↑, ↓↓↓) and the stability of each target depends solely on the state of its two neighbors. (While 2 neighbors are considered here as AF-lines are used as a case study, this approach could be extended to N neighbors to consider majority gates, fanout, etc.)

We use OOMMF to measure the fringing fields that a target magnet could experience to determine how the EB – and hence stability – of a target magnet might be impacted by neighboring device state. Assuming an initial/desired ↑ or ↓ state for a target device, we consider the impact on the EB between the initial/desired state, and the opposite/mistake state when the target is subjected to fringing fields from two neighbors in every possible magnetization state. Device angles between ±90º, in 1º increments are considered (resulting in 32,761 possible magnetization states), and average fields are measured *x* nm away from the simulated neighbor device to account for device-to-device spacing in a circuit. (This data could be reused if one were interested in the effects of different spacing between devices.)

We then calculate the EB of the target magnet (in isolation), which can include energy from shape anisotropy (demagnetizing energy) and crystalline anisotropy (to be discussed in Sec. 5). This curve includes angles between ±90º, in 0.1º increments (1801 total data points), and requires ~30 minutes of simulation time. This data is used to determine the "net" EB of the target (the base EB of the target plus the energy from neighboring devices). This combined EB curve is then used to quantify target stability (the EB between a desired state and a mistake state) for each of the 32,761 possible neighbor states described above.

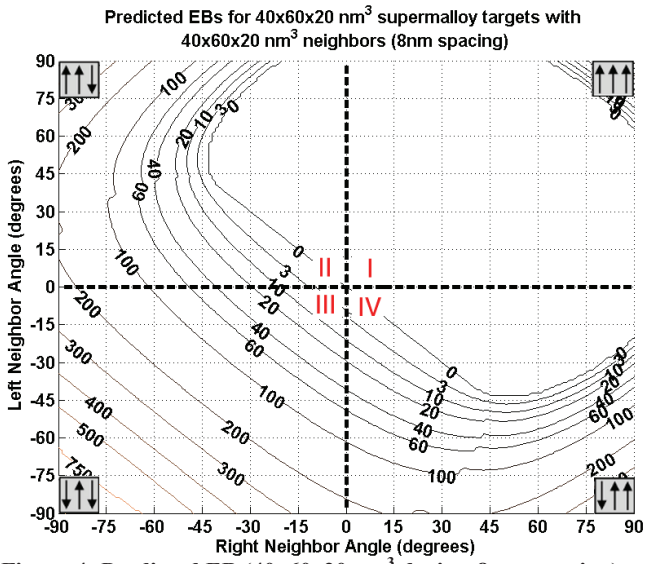

Figure 4: Predicted EB (40x60x20 nm^3 device, 8 nm spacing).

As an example, assume the desired state of the target is such that M_y is positive (i.e., +90º or ↑). Beginning at +90º, we sweep the EB curve from +90º to -90º until we either (i) encounter a local energy minimum, or (ii) reach -90 degrees and encounter no minimum. This local minimum represents the state the target would change to if it begins with +M_y (↑) and is subjected to the fields from the neighbors.

There are now three possible cases to consider. **First**, the local minimum is such that M_y is negative, which suggests the target would undergo a state transition to a state such that the y-component of magnetization would be negative (↓). In this case, the EB is predicted to be 0. **Second**, if the local minimum is associated with a positive angle (i.e., such that M_y is still positive), and there exists another minimum (found by sweeping the curve starting from *this* minimum to -90º), the EB is the height of the curve between these two minima. **Finally**, if the local minimum is associated with a positive angle, but there is no other minimum, we consider the EB to be the difference between this minimum and -1º (i.e., the energy to transition from ↑ to ↓). The net result is a stability prediction for all possible neighbor states.

The contour plot in Fig. 4 is a visual representation of the data generated by the process described above for the core of the AF-line in Sec. 3.1 (i.e., three, 40x60x20 nm^3 devices with 8 nm spacing). (Lines are representative of 'N' in N kT, for T=300K.) The magnetization state described by quadrant I represents a true worst case when considering the stability of a line of magnets. We would like a target to retain a positive, y-component of magnetization (↑), but fringing fields from both neighbors are directed in the opposite direction. While statistically unlikely, this case could occur if random walks from two adjacent clock groups migrate to a device in a middle group. A bit flip is all but certain, as our model predicts essentially no stability in this quadrant.

Quadrants II and IV represent "architectural conflicts," and suggest that if the angle of magnetization of neighboring devices is approximately +45º/-45º (left/right in quadrant II), the probability of a state transition is ~13% per ns (predicted EB is 2). (By Arrhenius-Neel theory of thermally activated magnetization reversal, the probability per unit time of reversal over the EB is $1/\tau$, where $\tau = t_o \times \exp(EB/k_bT)$, and t_o is the time for a thermally activated reversal – assumed to be 1 ns per [20]). Notably, 0K simulations of the same line suggest that, due to additional fringing field coupling associated with 8 nm device spacing, the angle of magnetization of each device in an *AF-line with no conflicts* is approximately ±45-50º. (Experiments in [21] also suggest increased ferromagnetic ordering at closer spacing.) This explains the random walk described in Sec. 3.1. Additionally, per supplement Sec. S1, thicker devices in line ensembles can require lower clock fields because of increased device-to-device coupling.

Finally, quadrant III represents the case where there is no conflict, and a line is completely AF-ordered. Given the ~200 kT stability, information should be retained (fringing fields from neighboring devices reinforce a target's state even when at ±45-50º angles).

In the context of these contour plots, we note two approaches to provide N kT stability in a circuit. **First**, one can mitigate conflict migration if the desired N kT stability is achieved for all points in quadrants II and IV for all magnets, as the worst case (quadrant I) should not occur. **Second**, if the stability of selective "latch" magnets (see Sec. 4) is at least N kT in quadrant I; random walks would be allowed in the remaining, unstable magnets, and the latches would preserve state. (See Sec. S2 for additional discussion of this case.)

Finally, we note that our method for quantifying stability could trend toward the pessimistic (we assume static neighbor state, whereas thermal noise may only result in the worst case for a relatively short time). However, it may be possible to relax our model. For example, Fig. 4 suggests that if the angle of magnetization for the left and right neighbors is sufficiently restricted in the steady state, the ensemble will remain stable. (See supporting data for this assumption in Sec. 4.) For example, per Fig. 4 (quadrant II) if the final magnetization states of the left and right neighbors did not deviate beyond +60º and -60º respectively, the probability of the target flipping in a given year is ~2.8×10^{-10}, and in our first approach we would not need to design for N kT for *all* angles in quadrants II, IV.

4. IMPROVING NON-VOLATILITY

Here, we explore ways to tune EBs in polycrystalline devices for improved stability. Lowering inter-device coupling effectively raises the energy barrier of each device, e.g., compare EBs in Fig. 2e where a device couples with 1 neighbor vs. 2b where it couples with 2 neighbors. Coupling can be decreased by increasing inter-device spacing, decreased device thickness (see quantitative discussion in Sec. S1), or changing magnet shapes. Alternatively, raising the intrinsic EB of each device can increase ensemble stability. The EB is proportional to the demagnetizing factor, volume, and saturation magnetization of a magnet. Thus the EB can be raised by, for example, increasing device aspect ratio, volume, or tuning device EB with different materials.

We now present two test cases where we leverage aspect ratio alone to demonstrate the two approaches for improving steady state stability (over the original design in Sec. 3.1). The discussion is not intended to represent an exhaustive study, but rather to identify design options that should be explored to achieve the best balance between low energy clocking and non-volatility. Any potential increases to clock energy are also captured quantitatively. (Additional levers are considered in Sec. 5.)

4.1 Approach 1: Eliminate Random Walk

An obvious first attempt to improve stability is to raise the EB of all devices in an ensemble by increasing their aspect ratio. Improved stability can be explained by considering the demagnetizing energy of a given device – illustrated as a function of angle of magnetization for 40x60x20 nm^3 and 40x80x20 nm^3

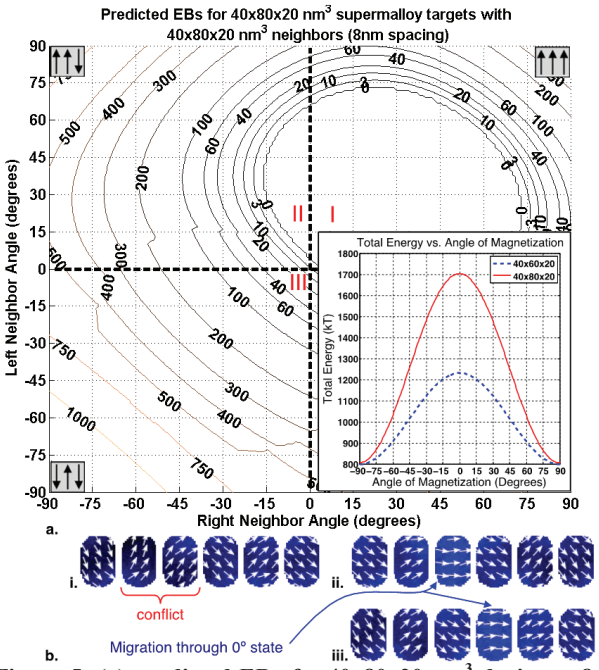

Figure 5: (a) predicted EB of a 40x80x20 nm^3 device at 8 nm spacing; (b) snapshots of random walk in 40x60x20 nm^3 line.

devices at 300K in the Fig. 5a inset. As the aspect ratio of a device increases, the energy required for a magnet to transition to a 0º state also increases. This is especially important as the state-changing random walks that occurred in the line of 40x60x20 nm^3 devices were facilitated by a transition through a lower energy, F-ordered state (Fig. 5b). Given the higher/steeper energy landscape for the 40x80x20 nm^3 device (Fig. 5a inset), hard axis directed fringing fields that can impact stability should be less significant.

As expected, lines of 40x80x20 nm^3 devices could be quite stable even if conflict states occur. With one conflict (quadrants II, IV in Fig. 5), if devices remain magnetized along their easy axes, an EB of >500 kT is predicted. Micromagnetic simulations (and the energy landscape in Fig. 5a) reinforce this assertion, as the average angle of magnetization observed for the configuration captured by quadrant II is not less than ±86º (averages of 0K and 300K simulations sampled over 40ns.).

However, not surprisingly, the clock energy required to re-evaluate an ensemble will increase. Simulations suggest that required fields will increase from 5 mT (for a line of 40x60x20 nm^3 devices) to 50 mT (for a line of 40x80x20 nm^3 devices). As the magnitude of a current generated field is directly proportional to the current (i.e., B ~ μI), and line energy is a function of I^2, Ohmic losses would increase by a factor of 100. Studies of reduced aspect ratio devices (40x70x20 nm^3) suggest that AF-lines can be re-evaluated with a 25 mT field (Ohmic losses would increase by 25), and could be sufficiently stable (e.g., 500 kT with angles of ±83º as observed in simulation). However, additional tuning of aspect ratio could be impeded by lithographic resolution, as only 10 nm of "height" remain (to 40x60 nm^2 footprints).

4.2 Approach 2: Selective Latching

As suggested in Sec. 3.2, not all devices within a clock group must be non-volatile in order to preserve pipe stage state. Instead, we can preserve information within a pipe stage by improving the steady state stability of select "latch" devices. One approach is to selectively introduce higher AR devices within a clocked segment (i.e., the *'ed magnets in Fig. 3c). For example, one might consider a line of 40x60x20 nm^3 devices where select devices are replaced by higher aspect ratio, 40x80x20 nm^3 devices. Regarding fabrication, this would not be challenging, as all devices could still be made with a single mask.

Regarding stability, our analysis suggests this latch should increase stability in quadrant I by an average of 83X (compare contour in Sec. S3, Fig. S1 to Fig. 5). When considering clock energy, higher fields were still needed to move data through the higher aspect ratio device during re-evaluation. However, we can modify the waveforms associated with a three-phase clock such that the first phase now operates at 50 mT (to place latches in a 0º state), and the second phase operates at 5 mT (to clock the low-AR devices). Simulations show that this facilitates data movement through the line. Total energy is thus increased by a factor of 50X. Again, lower aspect ratio, 40x70x20 nm^3 latches could operate with 5mT/25mT fields (leading to an energy increase of 13X and an average stability increase of 19X in quadrant I). While better than Sec. 4.1, the increase in clock energy is still significant.

5. LOWER ENERGY ALTERNATIVES

Work in Sec. 4 suggests that pipelined, polycrystalline magnet ensembles can be engineered to be NV, but that clock field requirements for re-evaluation could become unacceptably high. Here, we discuss additional (materials centric) approaches for low energy clocking of field driven, NV NML circuits.

5.1 Enhanced permeability dielectrics

As suggested in [2] the ratio of flux density to magnetic field strength (μ=B/H) could be increased by surrounding devices with superparamagnetic CoFe magnetic nanoparticles (~2-5 nm in diameter) [11]. Switching currents could be reduced by a factor of μ_r, and I^2R losses by μ_r^2. Recently, we have reproduced EPD films in [11], and are now working to integrate NML devices. Preliminary films demonstrate relative permeabilities of ~4.5. This could improve clock energy by ~20X – although EPDs may increase steady-state device-to-device coupling as well. (EPDs / new experiments are discussed further in Sec. S4.)

5.2 Biaxial anisotropy

Devices with biaxial anisotropy ([9]) were proposed to increase hard axis metastability during ensemble re-evaluation, and make *soliton*-based switching more reliable. (For a detailed discussion of soliton-based operation and a comparison to our approach, see Sec. S5.2.) Recently, devices with biaxial anisotropy were added to our design space exploration efforts, which emphasize the identification of device features to minimize field-based clock energy. Initial results – presented here for the first time – are encouraging, and could impact both clock energy and stability.

Consider first micromagnetic simulations of AF-lines comprised of 5, 60x90x5 nm^3 devices spaced 10 nm apart. The material parameters chosen were essentially identical to those used in [10], (see Sec. S5.4). Also, a detailed discussion justifying the use of devices with a larger footprint appears in Sec. S5.6 – but recall that random walks in lines with devices with the same footprint and spacing were also observed. With K_1 equal to 15 and 30 kJ/m^3, a 10 mT field is sufficient to re-evaluate the AF-ordered line with a new input (see Fig. S6a for 30 kJ/m^3 data). Per Sec. S5.5, additional energy reductions appear possible (via additional field reductions to 7.5 mT or alternative clock waveforms). In identical lines with K_1 = 0 kJ/m^3, signal propagation failed in 8 of 10 different simulations (to capture effects of thermal noise) – *even when a 15 mT clock field was employed.*

These trends can be explained by considering the energy landscapes for the biaxial device (K_1=15 kJ/m^3) and polycrystalline device (K_1=0 kJ/m^3) when each device is subjected to a 33 mT field in the 0º direction. (The devices are otherwise similar.) This field is representative of (i) the fringing fields produced by two neighboring devices on a target (~28 mT with 10 nm spacing between devices) and a 5 mT clock field. If we assume that each device originally had a positive, y-component of magnetization, the energy landscape (see Fig. S5a) suggests the biaxial device will transition to the metastable state (for re-evaluation), while the polycrystalline device would retain some of its state. (Dynamic simulations in Sec. S5.7 also show this.)

While biaxial anisotropy has the potential to benefit *all* NML ensembles – especially if devices are thinned for integration with I/O structures (see [8, 21] and Sec. S5.6) – additional analysis suggests that we can also use it to improve steady state stability. As device thickness decreases, the magnetization state of an individual device is more aligned along its easy axis (toward ±90º) as a result of less x-directed coupling. Per Sec. 4, this should help to improve stability, while the biaxial component could help to keep clock energy low (see Fig. S5a).

Consider the case of 3, 60x90x5 devices (K_1=15 kJ/m^3) spaced 10 nm apart (see Fig. S5b for contour plot of data). Our analysis suggests that if the angles of magnetization of the left/right neighbor do not move beyond +75º/-75º respectively, the probability of architectural conflict migration is low (the predicted EB is > 60). (Simulation data sampled over ~5 ns suggests the angle of magnetization does not deviate by more than -86.6º for the left neighbor, and 85º for the right neighbor.) Finally, simulations to quantify clock field requirements of 60x90x30 nm^3 devices with 10 nm spacing, and where random walks *were* observed, suggested that 5 mT fields were needed for re-evaluation. Simulations of biaxial ensembles (including those that were pipelined) suggest that 7.5-12 mT fields are needed to re-evaluate – which would lead to a net increase in clock energy of ~2.3-5.8X with no enhancements. This merits further study.

6. SUMMARY AND CONCLUSIONS

In this paper, we have explained how architectural-level bit conflicts can occur in defect free NML ensembles, and said conflicts can make supposedly NV circuits volatile. When studying magnet ensembles proposed in previous work [2] – that could be re-evaluated with clock fields that would offer energy savings over state-of-the-art low power CMOS – we found that pipelined circuits would *not* retain their state post re-evaluation. To combat this problem, we first developed a methodology for quantifying ensemble stability, and showed that properly designed, 3-magnet ensembles can mitigate volatility introduced by architectural-level conflicts. Moreover, while our work primarily focused on experimentally demonstrated, field-based clocking, the conflicts described in this paper will occur in any pipelined NML circuit, regardless of what clock is employed. As such, our tools should be applicable to other clocking approaches as well – e.g., as tighter device spacing might be required to help preserve hard axis metastability in soliton-based switching with a multiferroic clock. When discussing design alternatives to improve the stability of polycrystalline ensembles, we identified what the NML design space must "deliver" to ensure non-volatility. However, increased clock energy or fine-grained lithography may be needed. We concluded by discussing materials-related design levers. Most notably, biaxial anisotropy could minimize clock energy in *any* NML circuit (especially when considering integration with I/O). An added benefit appears to be improved steady state stability. Future work will further investigate this space (and other NML circuit constructs) to significantly narrow the design space for temperature-accelerated experiments to further study non-volatility.

7. REFERENCES

1. Chandrakasan, A.P., et al. Technologies for Ultradynamic Voltage Scaling. *Proceedings of the Ieee*, *98* (2). 191-214, 2010.
2. Dingler, A., et al. Performance and Energy Impact on Locally Controlled NML Circuits. *ACM Journal on Emerging Technologies in Computing*, *7* (1). 1-24, 2011.
3. Abelson, L.A., et al. Superconductor integrated circuit fabrication technology. *Proceedings of the Ieee*, *92* (10). 1517-1533, 2004.
4. Guo, X., et al. Resistive computation: avoiding the power wall with low-leakage, STT-MRAM based computing. *Proc. of 37th Int. Symp. on Comp. Arch. (ISCA)*. 371-382, 2010.
5. Matsunaga, S., et al. Fabrication of a Nonvolatile Full Adder Based on Logic-in-Memory Architecture Using Magnetic Tunnel Junctions. *Applied Physics Express*, *1*. 091301, 2008.
6. Mochizuki, A., et al. TMR-Based Logic-in-Memory Circuit for Low-Power VLSI. *IEICE Trans. Fundam. Electron. Commun. Comput. Sci.*, *E88-A* (6). 1408-1415, 2005.
7. Crocker, M., et al. Design and Comparison of NML Systolic Architectures. *IEEE NANOARCH*. 29-34, 2010.
8. Niemier, M.T., et al. Nanomagnet Logic: Progress Toward System-Level Integration. *J. Phys. Con. Mat.*, *23*. 493202, 2011.
9. Carlton, D.B., et al. Simulation Studies of Nanomagnet-Based Logic Architecture. *Nano Letters*, *8* (12). 4173-4178, 2008.
10. Carlton, D.B., et al. Computing in Thermal Equilibrium With Dipole-Coupled Nanomagnets. *IEEE TNANO*, *10* (6). 1401-1404, 2011.
11. Pietambaram, S.V., et al. Low-power switching in magnetoresistive random access memory bits using enhanced permeability dielectric films. *App. Phys. Let.*, *90*. 143510, 2007.
12. Pulecio, J.F., et al. Magnetic cellular automata coplanar cross wire systems. *J. of App. Phys.*, *107* (3). 034308, 2010.
13. Imre, A., et al. Majority logic gate for Magnetic Quantum-dot Cellular Automata. *Science*, *311* (5758). 205-208, 2006.
14. Niemier, M.T., et al. Clocking Structures and Power Analysis for Nanomagnet-Based Logic Devices. *Int. Symp. on Low Power Elec. and Design (ISLPED)*. 26-31, 2007.
15. Alam, M.T., et al. On-Chip Clocking for Nanomagnet Logic Devices. *IEEE Transactions on Nanotechnology*, *9* (3). 348-351, 2010.
16. Alam, M.T., et al. On-chip Clocking of Nanomagnet Logic Lines and Gates. *to appear in IEEE TNANO*, 2011.
17. Chu, Y.H., et al. Electric-field control of local ferromagnetism using a magnetoelectric multiferroic. *Nat. Mat.*, *7* (6). 478-482, 2008.
18. Salehi, F.M., et al. Magnetization dynamics, Bennett clocking and associated energy dissipation in multiferroic logic. *Nanotechnology*, *22* (15). 155201, 2011.
19. Donahue, M. OOMMF User's Guide, Version 1.0, Interagency Report NISTIR 6367.
20. Rizzo, N.D., et al. Thermally activated magnetization reversal in submicron magnetic tunnel junctions for magnetoresistive random access memory. *App. Phys. Let.*, *80* (13). 2335-2337, 2002.
21. Lyle, A., et al. Probing dipole coupled nanomagnets using magnetoresistance read. *J. App. Phys.*, *98* (9). 092502, 2011.

Paper Supplement

1. DEVICE THICKNESS

Intuitively, assuming a constant aspect ratio, as both the volume and demagnetizing factor N_d are roughly proportional to the thickness of a device, the energy barrier (EB) (and thus stability) of an individual magnet decreases with the square of the thickness. Thus, in isolation, thinner devices should (i) require lower fields to flip, (ii) require lower fields to hard axis bias, and (iii) be less stable.

In previous design space exploration efforts [1], the trends described by items (i) and (ii) were also observed when considering the magnitude of the clock field required to re-evaluate ensembles of devices of varying size, aspect ratio, thickness, etc. For example, fields needed to saturate (such that $M_x = M_s$) a line of 40x60x20 nm^3 devices spaced 16 nm apart were ~10% higher than those needed to saturate a line of 40x60x10 nm^3 devices with the same spacing. However, as spacing was decreased, these trends were *reversed*. As a result of increased device-to-device coupling, clock fields required to saturate the line of 10 nm thick devices spaced 8 nm part were ~17% *higher* than those needed for a line of 20 nm thick devices.

2. DESIGN POINT DISCUSSION

Using Fig. 3c in the main manuscript as context, assume there is a power failure when devices in the switching and buffer groups are in the metastable, 0º state. If these devices relax randomly, the situation described by quadrant I could occur. The latch could preserve state in the un-clocked driving group. If we simply save the current clock period in non-volatile memory – just 2 bits would be required – computation could be restarted.

3. LATCH STABILITY

Fig. S1 depicts the stability of the 40x80x20 nm^3 latch magnets with 40x60x20 nm^3 neighbors (discussed in Sec. 4.2 of the text).

4. EPDs

Enhanced permeability dielectrics (EPDs) with embedded magnetic nano-particles (e.g., CoFe particles 2-5 nm in diameter) were proposed in [2] to increase the field from a word or bit line in field MRAM without increasing current. The authors suggest that absolute permeability ($\mu = \mu_o \times \mu_r$) could improve by as much as 30X, although μ_r's of 2-6 were most common experimentally. As illustrated in Fig. S2, we have reproduced the films described in [2], and are now working to integrate NML devices.

As a representative example, a film comprised of 6-to-9 nm diameter CoFe particles appears in Fig. S2a. Vibrating sample magnetometer (VSM) characterization (Fig. S2b) suggests that (i) this film has a relative permeability of ~4.5 (determined by measuring the slope of the low field magnetization data – as was done in [2]), and (ii) that the particles are superparamagnetic (no coercivity or remanence was observed). Notably, this "boost" to μ_r could improve clock energy by ~20X – although EPDs could also increase device-to-device coupling as well. How this affects stability remains to be investigated.

5. BIAXIAL ANISOTROPY

5.1 Concept

Depending on its value, the biaxial anisotropy term flattens and/or introduces a local minimum in the energy landscape of an individual magnetic island at the 0º point (see Fig. S3).

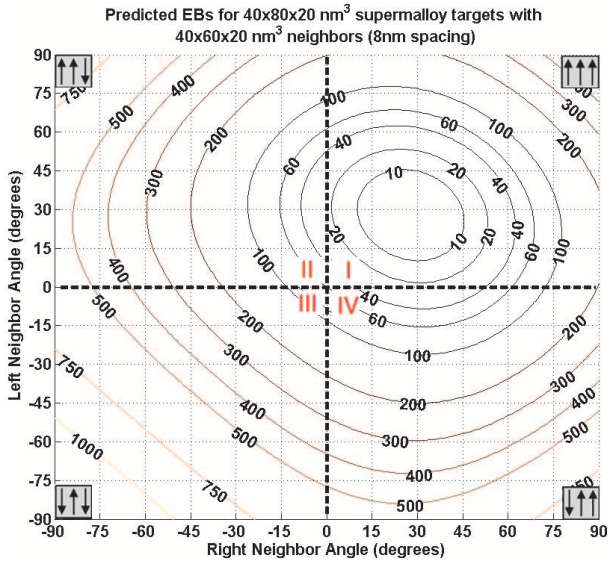

Figure S1: Stability of a 40x80x20 nm^3 latch neighbored by 40x60x20 nm^3 devices with 8 nm spacing.

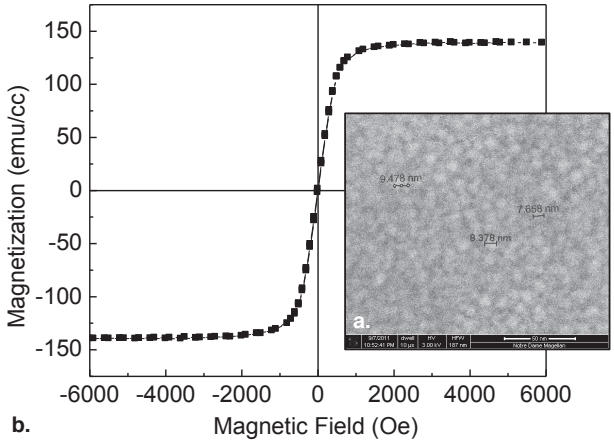

Figure S2: (a) SEM image of CoFe particles that comprise EPD film; (b) VSM characterization suggests μ_r is ~4.5.

5.2 Soliton-based switching

With soliton-based switching, all devices in a clocked ensemble are simultaneously placed into a 0º state. The clock field is then removed, and dipole fields from neighboring magnets alone are expected to preserve metastable, 0º-ordering until a device is set by an appropriate neighbor. To prevent premature switching due to thermal noise, [5] proposed devices with a magnetocrystalline biaxial anisotropy such that $U(\theta)$ becomes $K_u\cos^2(\theta) + \frac{1}{4}K_1\sin^2(2\theta)$ (K_1 is the biaxial anisotropy constant). The biaxial anisotropy term can impact the energy landscape of an NML device at the 0º point (e.g., per Sec. S5.1, Fig. S3, a local minimum can appear).

Although there are challenges to soliton-based switching, additional advantages could include further reductions in clock energy, as the clock could be turned off after ensemble metastability is achieved. In simulations described in Sec. 3 and Sec. 4 of the main manuscript, devices are biased into a new, logically correct state before an external field is removed.

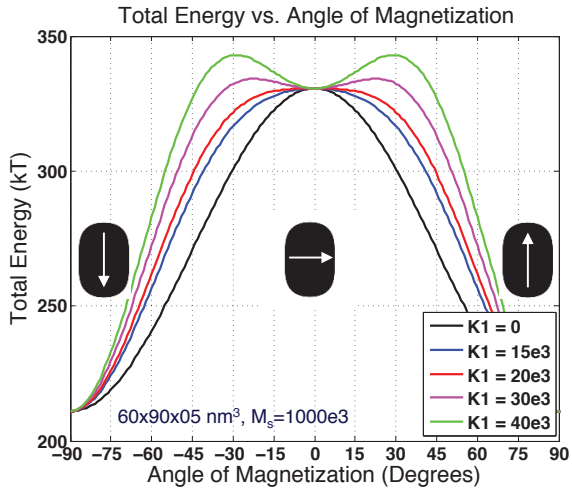

Figure S3: As K_1 increases, the depth of the local energy minimum at 0º increases as well. Per [1], the energy minimum must be tuned such that it is high enough to prevent premature relaxation, and low enough so that a neighbor can still bias a device to a new, and logically correct state.

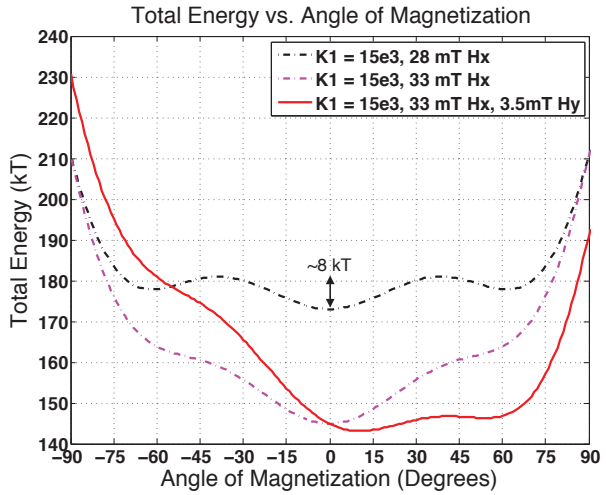

Figure S4: Representative energy landscape for a device in the middle of an anti-ferromagnetic line.

While this will (i) result in an increase in clock energy, and (ii) turn successive devices in a group into weaker drivers (eventually limiting the width of a clock line), potential advantages include a decreased likelihood of premature switching (as switching dynamics are similar to those described by Figs. 2b,c of the main manuscript where there is an absolute energy minimum). Performance wins projected by [3] account for this increased clock energy.

While a detailed discussion is beyond the scope of even this supplement, we believe that switching in the presence of an applied field could help to reduce error rates during the switching process (i.e., after a device ensemble has been placed into a metastable state). Briefly, assuming the soliton-based switching approach discussed at the beginning of this section, only device-to-device fringing fields preserve 0º, metastability during the re - evaluation process. For the devices considered in the simulations captured by Fig. S6, the average field that an internal device

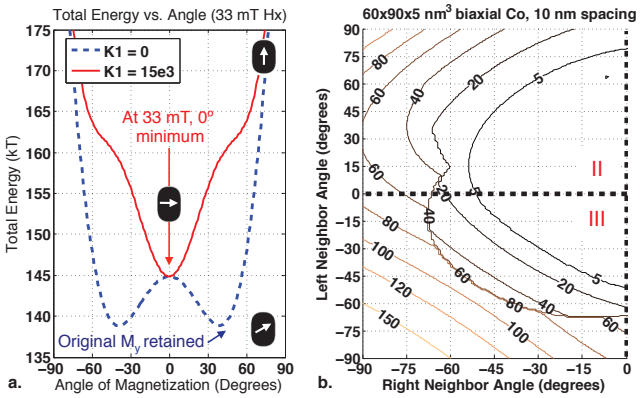

Figure S5: (a) energy landscape for polycrystalline, biaxial devices with 33 mT 0º field; (b) predicted EBs (quadrant II, III) for 60x90x5 nm^3 devices spaced 10 nm apart.

would experience from two nulled neighbors is approximately 28 mT. The energy landscape for a given device (subject to a 28 mT, hard-axis directed field) is illustrated in Fig. S4. While there is a local energy minimum at the 0º / metastable state, only an 8 kT barrier separates this metastable state from a potential mistake state. (As such, thermal noise, fabrication variation, etc. could induce a transition to a mistake state.) However, given a nominal clock field (e.g. 5 mT), the 0º / metastable state represents an *absolute energy minimum*. Moreover, given a y-bias (presumably from a neighboring device), any energy minima are on the logically correct side of the 0º point – suggesting that information can propagate through the ensemble in the presence of an applied field.

Additionally, in the simulation efforts in [4], the authors note that dipole-to-dipole coupling alone could be insufficient to keep an anti-ferromagnetically ordered line (for example) hard-axis-biased even if devices with biaxial anisotropy are employed. Thermal noise could induce premature, random, and unwanted switching. Thus, while appealing, the viability of true, soliton-based switching does need additional study.

5.3 Energy landscape and stability

Fig. S5a depicts the energy landscapes for polycrystalline and biaxial devices in isolation (with a field along the x-axis). Fig. S5b depicts the predicted EBs for 60x90x5 nm3 devices spaced 10 nm apart. Both figures are discussed in Sec. 5.2 of the main manuscript.

5.4 Material parameters

The material parameters chosen were essentially identical to those first proposed in [5] – i.e., as the saturation magnetization (M_s) is also 1,000,000 A/m. Additionally, as in [5], the exchange stiffness A was set at 13×10^{-11} J/m. One minor difference between our simulations and those in [5] is the damping parameter α – where a lower, more realistic value of 0.05 was used in our simulations instead of 0.1 used in [5]. Per [6], using even lower values requires additional reductions in simulation time step which can in turn make simulations excessively long. Additionally, differences in projected field requirements for device switching were negligible with lower damping coefficients (e.g., 0.01).

5.5 Simulations of biaxial, AF-lines

Here, we provide a more detailed discussion of simulations of biaxial, AF-ordered lines. Simulation setup is described, and representative results are illustrated graphically in Fig. S6.

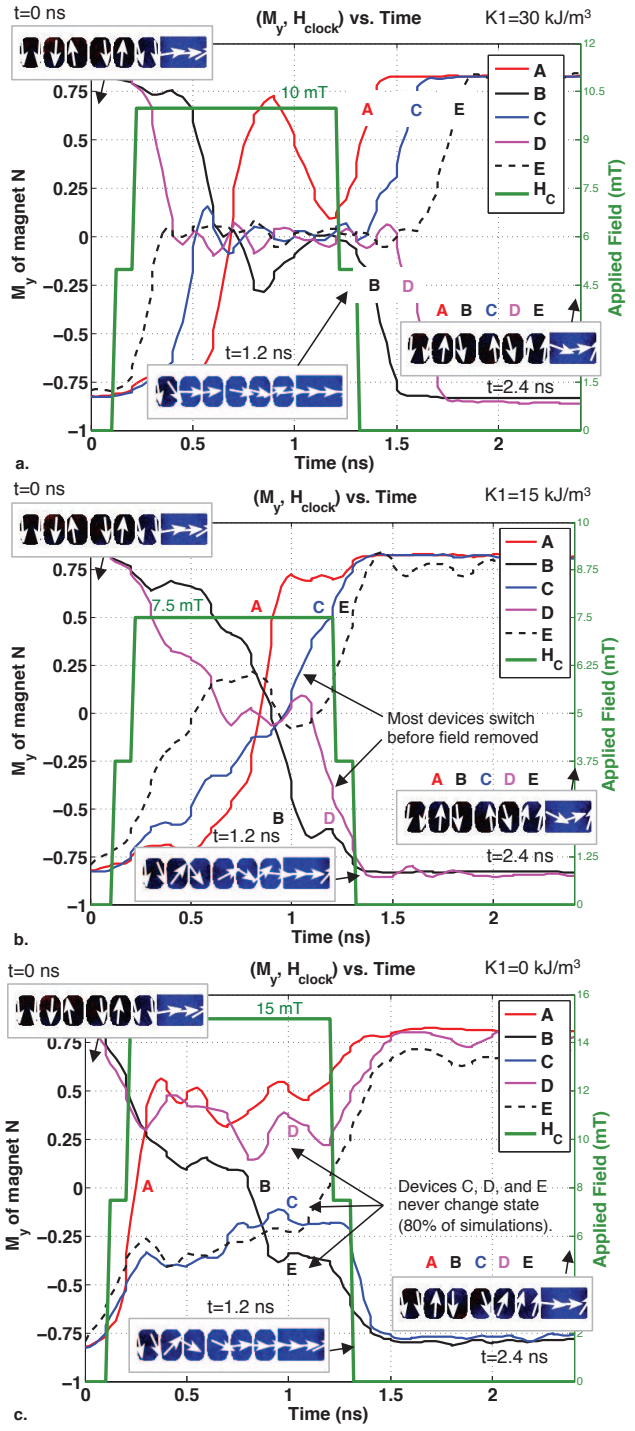

Figure S6: (a) Magnetization state (M_y) for every device (K_1 = 30 kJ/m^3) in an AF-ordered line as a function of time. When the applied field is removed, devices switch (in the correct order) to an AF-ordered state associated with a new input; (b) with K_1 = 15 kJ/m^3, fields of 7.5 mT can facilitate re-evaluation (40% success); (c) with no biaxial anisotropy, *15 mT* fields only facilitate re-evaluation in 2 of 10 cases.

Note that at the beginning of a simulation, the state of the input device has been flipped, while the remaining devices are in their previous, logically correct, AF-ordered state (see devices A-through-E in Fig. S6 insets). A 0º directed field was applied to this ensemble for 1.0 ns (increasing from 0 mT to a peak value in 0.2 ns). The hard axis clock field was then removed (transitioning from a peak value to 0 mT in 0.2 ns). The ensemble was then allowed to completely relax into a final/ground state for 1.0 ns. (Devices were only subjected to fringing fields from neighbors and thermal noise during this last window.) For all cases considered, 10 simulations were performed, each with a different random seed. (Our intention is not to make claims about the statistical reliabilities of line switching, but to ensure that a single result is not an artifact of a chosen seed.)

Figs. S6 a-c illustrate how the magnetization state of each device in the line changes as a function of time. The desired simulation outcome (post clocking) is for the remaining devices in the line to change state in accordance with the new/fixed input, in the correct order. With K_1 equal to 30 kJ/m^3, a 10 mT field is sufficient to re-evaluate the AF-ordered line with a new input (see Fig. S6a). When K_1 was reduced to 15 kJ/m^3, again, a 10 mT field was sufficient to facilitate the re-evaluation of an identical line (not shown). In both instances, assuming a 10 mT clock field, (i) all 10 simulations exhibited logically correct functionality and (ii) signal propagation occurred after the field was removed – i.e. in a soliton-like fashion.

How biaxial lines responded to *lower* clock fields was also studied. When K_1 was reduced to 15 kJ/m^3, a 7.5 mT field was sufficient to facilitate the re-evaluation of the line with a new input, and switching occurred in the presence of an applied field.

While the results illustrated in Fig. S6b suggest that (i) field reductions of 33% are possible by tuning K_1 and (ii) that switching can occur even in the presence of an applied field, we must note that when the results of 10 simulations were considered, 4 of 10 were successful. In all instances, the first device in the line did not flip. Again, while a detailed discussion is beyond the scope of this supplement, alternative clock waveforms – e.g. a shorter, higher magnitude 10 mT pulse, followed by a 5 mT pulse also produced desired switching dynamics with a 100% success rate (similar to the approach suggested in Sec. 4.2 of the main manuscript). This will be studied in future work.

That said, the obvious comparison to be made is to contrast the results discussed above with an identical line of devices with *no* biaxial anisotropy. Representative simulations results are illustrated in Fig. S6c (K_1 = 0 kJ/m^3). As one can see, even after being subjected to a 15 mT field, devices C and D never reach the metastable state required for re-evaluation, and retain their original state. (Device E – which couples to the terminating block – is biased into a 0º state. Its state change is a result of random thermal noise post field removal.) Note that 8 of the 10 simulations performed resulted in a final, incorrect state of the line. Thus, the addition of biaxial anisotropy at the device-level seems to result in lower energy clocks – at least when considering 5 nm thick devices.

5.6 Biaxial implementations and device sizes

Before discussing *why* the addition of biaxial anisotropy can help to lower clock energy, for completeness, we briefly address (i) manufacturability and (ii) other aspects of this design space.

Regarding manufacturability, additional conversations with the authors of [5] suggest that devices with K_1 values ranging from 0-50 kJ/m^3 could be engineered.

Regarding the design space itself, it is probably obvious to the reader that when considering the NML devices discussed in Sec. 4 (40x60x20 nm^3 polycrystalline supermalloy devices spaced 8 nm apart) and the devices discussed here (60x90x5 nm^3 biaxial cobalt

devices spaced 10 nm apart) that several aspects of an AF-line design have changed. We address these design differences in a more controlled fashion below.

First, while no graphical results are included, simulations of biaxial supermalloy devices (K_1 = 15 kJ/m^3, M_s = 800,000 A/m) exhibit similar trends to those that were illustrated in Fig. S6. For example, all 10 simulations of the 5 magnet AF-line studied exhibited correct, soliton-like signal propagation when subjected to a 7.5 mT clock field.

Second, while some simulations of thicker devices exhibited correct signal propagation, simulations also suggested that several, undesirable switching characteristics were possible. For example, consider a line of 60x90x20 nm^3 devices (10 nm spacing between devices, K_1 = 40 kJ/m^3, M_s = 1,000,000 A/m).

Simulations show (graphical results not included) that with the larger K_1 value, devices are almost too strongly coupled, and signal propagation proceeds slowly. (In essence, computational latency will increase.) Consider also a line of 60x90x30 nm^3 devices (10 nm spacing between devices, K_1 = 15 kJ/m^3, Ms = 1,000,000 A/m). Given this device configuration (again, graphical results not included), the first device in the line enters a relatively stable vortex state [7], and information never propagates down the line. The aforementioned issues were not observed with lines of thinner, biaxial devices.

Third, magnet thickness can impact chip-level energy dissipation. Each magnetic island will dissipate an amount of energy given by the EB between the hard and easy axes of the magnet. This can be tuned precisely by altering the aspect ratio, thickness, and saturation magnetization of the islands, as well as by adiabatic switching [8]. An upper bound on the energy dissipated by the magnets is then simply the number of magnets in a circuit ensemble (N) times the barrier height. The energy difference between magnetization states for the 60x90x5 nm^3 devices (~120kT) is more than an order of magnitude *less* that the energy difference between states for the thicker, 60x90x30 nm^3 devices (~2100kT). If we assume that 10^9 devices switch every nanosecond, the power dissipation from just the magnets could be ~17X higher (8.7W vs. 0.5W at 300K). As such, a shift to thinner devices can be favorable energetically.

Fourth, moving to thinner devices is also desirable from the standpoint of manufacturability – particularly when considering the integration of NML devices with structures to be used for the purposes of input and output. More specifically, [9] has proposed (and simulated) the use of magnetic tunnel junctions (MTJs) to provide magnetic-to-electrical and electrical-to-magnetic interfaces. For output, fringing fields from an NML device could be used to bias the free layer of an MTJ. The resistance of a given MTJ could then be sensed to determine whether an output of an NML ensemble is a 1 or a 0. For input, one could leverage spin transfer torque (STT) to set the state of an MTJ's free layer. Fringing fields from the free layer could then be used to set the state of successive devices in an NML ensemble.

That said, challenges to this approach include (i) whether fringing fields from a thinner free layer are of a sufficient magnitude to set the state of a thicker device (at the inputs), (ii) the use of STT to set the state of a (relatively) thick free layer, and (iii) the feasibility of integrating thinner devices (free layers) with thicker NML devices (as mask alignments would be required). As such, uniform device / free layer thickness is desirable from the standpoint of manufacturing NML ensembles that are integrated with needed I/O circuitry.

Finally, as noted in the main manuscript, random walks were also observed in thicker, polycrystalline devices with the same footprint and spacing

5.7 Dynamic data

Simulation results in Fig. S7 add further credence to the trends identified in Sec. 5 of the main manuscript. Here, identical, 60x90x5 nm^3 biaxial and polycrystalline devices are subjected to (i) a hard axis field that is increased in 1mT/100ps and 1mT/200ps increments and (ii) a constant, easy axis directed, 2 mT biasing field opposite to the original direction of magnetization (representative of a neighbor's fringing field). The biaxial device transitions to a new state (-M_y), through the 0º state in a non-linear fashion. There is no (binary) state change in the polycrystalline device.

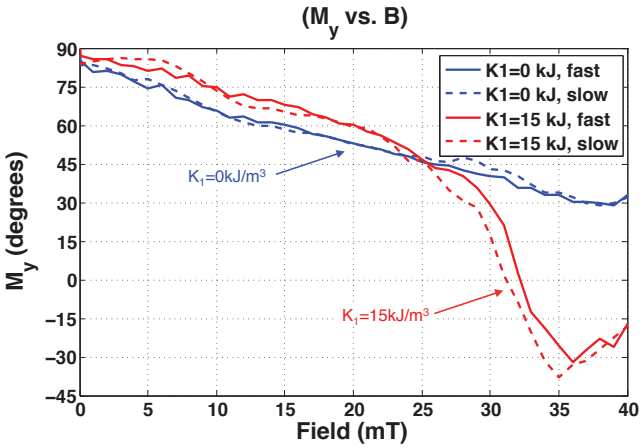

Figure S7: Switching dynamics of polycrystalline and biaxial devices when subjected to a 2 mT downward biasing field and a 0º field that increases in magnitude. The biaxial device experiences a state transition (with lower, 0º fields) while the polycrystalline device does not even change state.

6. REFERENCES

1. Niemier, M.T., et al. Nanomagnet Logic: Progress Toward System-Level Integration. *J.Phys.Con.Mat.*, *23*. 493202, 2011.
2. Pietambaram, S.V., et al. Low-power switching in magnetoresistive random access memory bits using enhanced permeability dielectric films. *App.Phys.Let.*, *90*. 143510, 2007.
3. Dingler, A., et al. Performance and Energy Impact on Locally Controlled NML Circuits. *ACM Journal on Emerging Technologies in Computing*, *7* (1). 1-24, 2011.
4. Spedalieri, F.M., et al. Performance of Magnetic Quantum Cellular Automata and Limitations Due to Thermal Noise. *IEEE TNANO, 10* (3). 537-546, 2011.
5. Carlton, D.B., et al. Simulation Studies of Nanomagnet-Based Logic Architecture. *Nano Letters*, *8* (12). 4173-4178, 2008.
6. Alam, M.T., et al. On-chip Clocking of Nanomagnet Logic Lines and Gates. *to appear in IEEE TNANO*, 2011.
7. Cowburn, R.P., et al. Single-Domain Circular Nanomagnets. *Physical Review Letters*, *83* (5). 1042-1045, 1999.
8. Csaba, G., et al., Power dissipation in nanomagnetic logic devices. in *IEEE Conf. on Nanotechnology*, 2004, 346-8.
9. Liu, S., et al. Magnetic-Electrical Interface for Nanomagnet Logic. *IEEE T. on Nanotechnology*, *10* (4). 757-763, 2011.